Structural characterization of GaN nanowires using TEM

Author: Daniel del Pozo Bueno.
*Facultat de Física, Universitat de Barcelona, Diagonal 645, 08028 Barcelona, Spain.**

Advisors: Gemma Martín and Francesca Peiro
(Dated: January 16, 2018)

Abstract: In the present study, gallium nitride (GaN) nanowires fabricated by top-down etching are investigated by transmission electron microscopy (TEM). The study starts with the lamella preparation using the lift-out technique in a focused ion beam (FIB) instrument. Subsequently, different observation modes of the TEM are applied to asses the quality of the growth and identify the crystal structure. Selected area diffraction mode (SAD) is used to obtain the diffraction patterns, which are appropriate to identify the crystal structure. Then, two-beam conditions are carried out to find the crystallographic defects and, finally, through the high resolution mode, the phase contrast images are used to achieve atomic resolution.

I. INTRODUCTION

Semiconductors of the group-III nitrides have interesting properties like band-gap energy from infrared to ultraviolet, high breakdown field and high electron saturation velocity [1]. This fact allows the building of devices with applications in optoelectronic and high power, high temperature, and high-speed electronics.

Gallium nitride (GaN) is a widely used semiconductor due to its high electron mobility, tunable band-gap and direct energy band-gap ($E_g = 3.4\ eV$). In particular, GaN nanowires (NWs) have multiple applications like solar cells [2], light emitting diodes (LEDs) [3], lasers [4] and photodetectors [5]. It is clear that GaN NWs are suitable for optoelectronic applications, which include the electronic devices and systems that can provide, detect and control light. The main reason for that is their high photosensitivity and photoconductive gain, which is the number of charge carriers that circulate through a circuit involving a photoconductor for each charge carrier generated by light.

Besides optoelectronic applications, the GaN NWs are also used for the fabrication of field-effect transistors (FET) [6, 7] where they offer some advantages for FETs such as large current densities per unit chip size, high-quality GaN non-polar surfaces without limitations from substrate lattice mismatch, efficient gate control and large driving current capability [7].

In this project, the GaN NWs, fabricated by top-down etching, have been characterized by the transmission electron microscopy (TEM). Different operation modes have been used to carry out a detailed characterization of the samples: the selected area diffraction (SAD) where the electron diffraction patterns of the sample have been obtained; the two beam bright field conditions to observed defects and, finally, the high-resolution mode (HRTEM) to achieve atomic resolution.

*Electronic address: ddelpobu11.alumnes@ub.edu

II. EXPERIMENTAL DETAILS

Two different samples have been studied, and hereafter they will be called C1 and C2. From bottom to top the samples are described as: a sapphire substrate, a buffer film of 100 nm of AlN and a film of 500 nm of GaN, where the NWs are found. The NWs were manufactured using a top-down fabrication method from the same GaN film [7, 8]. This method provides accurate control of either position and dimension of the NWs. The top-down technique has three conventional nanofabrication steps: electron-beam lithography, reactive-ion etching and wet-chemical etching. It was implemented identically to fabricate both samples with the same substrate (sapphire). Although the fabrication method was the same, the sample C2 was submitted to a rapid thermal annealing (RTA) process at 750°C, which consisted of heating a single substrate at a time in order to affect its electrical properties.

Different TEMs have been used for the characterization: the TEM JEOL 2010F operated at 200kV and equipped with a CCD $2k \times 2k$ and STEM–HAADF/BF detectors and the TEM JEM 2100 operated at 200kV, with a point resolution of $0.23nm$, and equipped with a CCD $4k \times 2.7k$ Orius (GATAN), STEM–HAADF detectors and an electron diffractometer, both located at the Scientific and Technological Centers of the University of Barcelona (CCiT). In the other hand, for the lamella preparation the focused ion beam (FIB) systems used have been the Helios Nanolab 650 double beam microscope of FEI Company equipped with Omniprobe micromanipulator (from SCBI-UMA) and the Focused Ion Beam Zeiss 1560XB CrossBeam (from CNM-IMB).

The CaRIne software has been run in order to index the diffraction patterns. The crystalline structures considered for the GaN have been acquired form the Crystallography Open Database. Also, the Gatan DigitalMicrograph software has been used to handle the images and perform geometrical measurements.

III. RESULTS

A. Sample preparation

In order to prepare electrotransparent thin lamellas (less than 100 nm), a FIB system has been used. The FIB is an instrument where charged particles are accelerated and focused using electric and magnetic fields. The FIB uses a beam of ions to directly modify or mill the sample surface, via an sputtering process. The milling is controlled with nanometric precision. The ion beam energy ranges between 5 keV and 30 keV and the beam intensity is regulated up to 10 pA. In addition, a chemical vapour deposition can be included to deposit material with a level of precision similar to FIB milling. The FIB is usually equipped with an electron gun, enabling dual beam operation and then scanning electron microscope imaging.

The samples have been prepared by the lift-out technique [9]. Although it is a standard methodology, the preparation is highly material-dependent and no universal procedure exists. So, a fair amount of adjustment and user interaction is needed for each situation. To summarize, our lamellas have been prepared using the following main steps:

Area selection and e-beam assisted deposition. The sample preparation starts selecting a convenient area and protecting it. The protection is relevant because the subsequent use of the FIB might damage the sample. We use a molecular gas with Pt and the e-beam assisted to deposit the protection layer. Firstly, the gas is injected in the chamber and through the ion beam, which breaks the gas molecules, the Pt deposits over the sample forming the Pt layer. The result is observed in the figure 1(a).

Trenches and U-cut. Once the sample is protected, it is time to use the FIB's ion-beam to cut the proto-lamella. Firstly, using two regular isosceles trapezoid patterns the FIB mills a trench on each side of the sample. It is important that those trenches are milled sufficiently deep below the area of interest of the sample, since we don't want to damage this region in future operations. After that, three rectangular patterns are used to cut the proto-lamella with an U-shape cut, which almost separates the proto-lamella from the bulk. So, while one side is completely separated from all the sample, the other is still connected through a bridge on the top. The proto-lamella in this stage is observed in the figure 1(b).

Lift-out and transfer. In order to transfer the proto-lamella to the TEM's grid, this one is attached to the tip of a nanomanipulator using Pt deposition. Once the remaining connection with the bulk is cut, the proto-lamella is ready to be lifted out and transported by the manipulator to an special FIB Cu grid and attached to one of its arms by Pt deposition. Then, it is detached from the manipulator by Ga etching. An example of proto-lamella fixed at the grid is shown in the figure 1(c).

Thinning. This is the final step to make the proto-lamella electrotransparent. Thus, we thin the proto-lamella until it is about tens of nanometres thick. And, now the lamella is ready to be examined by the TEM. The final result of the lamella for the sample C2 is observed in Figure 1(d).

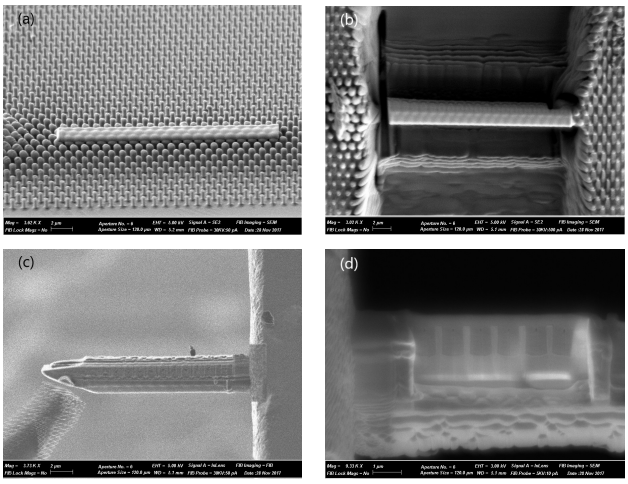

Figure 1: SEM images of different steps of the lamella preparation by the lift-out technique (sample C2). (a) Pt protection layer over the GaN NWs. (b) Proto-lamella with the trenches and the U-cut done. (c) Proto-lamella attached in the TEM's grid. (d) Final result of the lamella.

B. TEM for structural characterization

Transmission electron microscopy [10] is based on the interaction of energetic electrons with the sample to provide morphological, compositional and crystallographic information. The basic components of a TEM are: an electron emission system for the generation of the electron beam, an electromagnetic condenser lens system that focus the beam on the sample, an electromagnetic objective lens system which collects all the electrons after interacting with the sample and forms an image of it, the apertures which are annular metallic plates that exclude the electrons that are further than a fixed distance from the optic axis, a magnification system which is formed by a set of intermediate lenses that magnify the image and projects them on a phosphorous screen or a charge coupled device (CCD) and the data recording system. A vacuum system is also required to obtain a high vacuum conditions ($0,01$ Pa). The sample is located at the middle of the polar piece of the objective lens. The fundamental operation modes of the TEM are: bright-field (BF) and dark field (DF) imaging, which form images using just the transmitted beam or a diffracted beam, respectively; we have used those operation modes to measure the dimensions of the NWs, diameter, height and distance between them. The Figure 2 is an example of this BF imaging mode.

The results obtained for the dimensions of the NWs for both samples are: 950 ± 10 nm of height, 223 ± 5 nm of diameter and $1,02 \pm 0,01$ μm of distance between NWs.

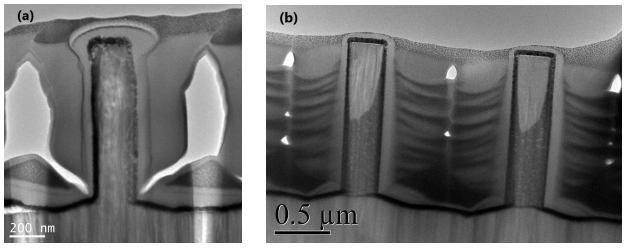

Figure 2: Bright field TEM images of the GaN NWs. (a) Sample C1. (b) Sample C2.

C. Diffraction patterns analysis

Bragg diffraction patterns give information of the three-dimensional periodic structure of atoms in a material, that is, the crystallographic lattice. Thus, diffraction patterns are very appropriate to deduce the crystalline structures and to assess the quality of the material. Then, by means of the selected area diffraction (SAD) technique the diffraction patterns of the samples have been obtained. They are a consequence of the Bragg's diffraction which occurs when electrons, with the de Broglie wavelength comparable to atomic spacings, are scattered in a specular fashion by the atoms of the crystalline system, and undergo constructive interferences. The scattered waves interfere constructively when the difference between path lengths of two waves is equal to an integer multiple of the de Broglie wavelength. Then, the measurement of path difference is $2d\sin\theta$, where d is the interplanar distance and θ the scattering angle. To summarize, the constructive interference occurs when $2d\sin\theta = n\lambda$, where λ is the incident electron wavelength and n is an integer. This diffraction condition is called Bragg's law.

Finally, to understand the diffraction patterns it is necessary to talk about the reciprocal lattice and the Ewald sphere. The reciprocal lattice is a construction where each set of parallel atomic planes, expressed by a vector $g_{hk\ell} = (hk\ell)$, is represented by a single point or spot in the lattice. In the other hand, the Ewald sphere is a sphere of radius $1/\lambda$ which determines the intensity value of every spot of the reciprocal lattice. Thus, if a vector, $g_{hk\ell}$, intersects with the Ewald sphere, the intensity is maximum, while, if it suffers a little deviation with respect to the sphere, the intensity is reduced.

Figure 3 shows the Bragg diffraction patterns of the crystal structure for both samples, which shows a good quality of the crystal lattice. The most stables crystallographic structures for the GaN are wurtzite, which is an hexagonal crystal system, and zinc-blende, which is a cubic crystal system. Considering the diffraction patterns obtained for the samples, they are in correspondence with the diffraction patterns expected for a hexagonal structure. Concretely, the measurements of distances and angles fits with the wurtzite structure.

The Miller-Bravais indexing system has been used for the indexation. This system is very suitable to index

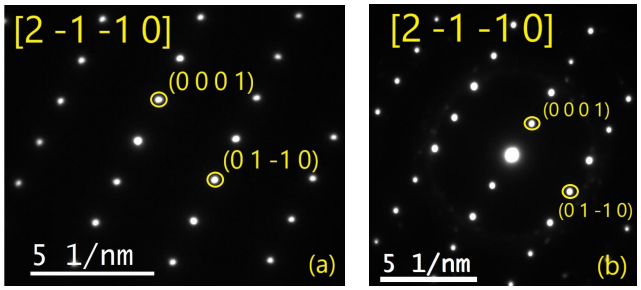

Figure 3: Indexed electron diffraction of the samples. (a) Sample C1. (b) Sample C2.

hexagonal crystal systems because this notation highlights the symmetry of the hexagonal crystal structure and allows to clearly distinguish those family of planes and directions which are equivalent through symmetry relations. It is a system formed by 4 index, $(hki\ell)$, where $i = -(h+k)$ and represent the coefficients of a vector $g_{hkil} = ha_1 + ka_2 + ia_3 + \ell c$, where $a_3 = -(a_1 + a_2)$ and a_i and c are the vectors represented in the Figure 4.

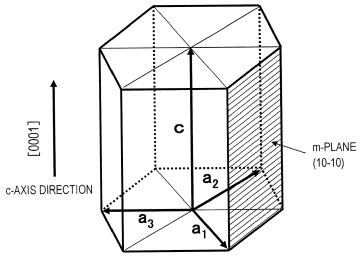

Figure 4: Axes for an hexagonal indexing system.

Through the diffraction patterns the interplanar distances can be calculated measuring the distance of the spots to the transmitted beam, once the camera length of the microscope has been correctly calibrated. Further, measuring the angles between the spots, the most suitable zone axis can be estimated using CaRIne database. The results are shown in Table I and the zone axis has been found to be $[\bar{1}\ 2\ \bar{1}\ 0]$. Therefore the NW growth direction is [0 0 0 1] as expected from the fabrication process.

Finally, although the spot [0 0 0 1] should be forbidden in this $[\bar{1}\ 2\ \bar{1}\ 0]$ view because of structure factor extinction rules, it is seen thanks to the double diffraction effect occurring when a diffracted beam becomes a "pseudo new incident beam" due to multiple scattering.

Interplanar distances		
Family of planes:	$\{0\ 0\ 0\ 1\}$	$\{0\ 1\ \bar{1}\ 0\}$
Sample C1 (nm)	5, 382	2, 846
Sample C2 (nm)	5, 142	2, 751
Theoretical results (nm)	5, 125	2, 725

Table I: Interplanar distances.

D. Two-beam analysis

Two-beam conditions operation mode enhances contrast defects. As has been commented previously, diffraction according to Bragg's law occurs whenever the Ewald sphere touches a point on the reciprocal lattice. Then, two-beam conditions are satisfied when the reciprocal lattice is rotated by appropriate double inclination (on x and y), so that a particular diffraction vector, $g_{hk\ell}$, is brought exactly on the Ewald sphere. That makes this particular diffraction spot as intense as the central beam. So, only the [0 0 0] and $[hk\ell]$ directions are on the Ewald sphere. As a result, the other directions moves even farther away from the Ewald sphere resulting in significant decrease in their intensities. Under quasi two-beam BF conditions, the dislocation is shown as a dark line on a bright background. This is because strong diffraction occurs close to the dislocation core, where the crystallographic planes are bent and Bragg law is fulfilled, whereas the aperture selects only the transmitted beam to form the image.

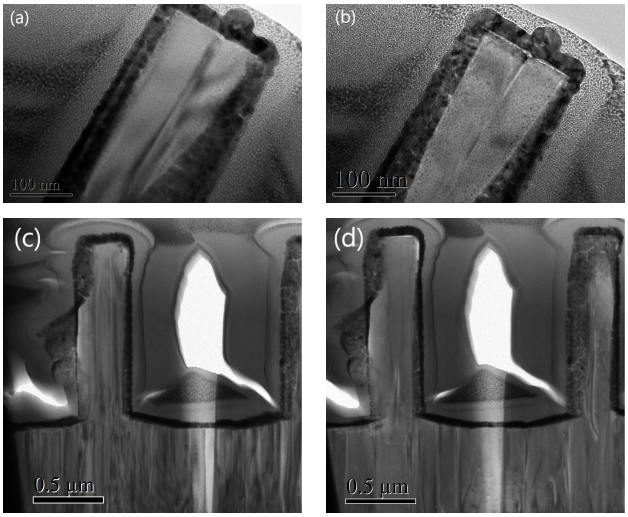

Figure 5: Pairs of BF images under two-beam conditions assessing the presence of threading dislocations. Images (a), (b) correspond to sample C1 and images (c), (d) to sample C2. The perpendicular vectors for the two beam conditions are: [0 1 $\bar{1}$ 0] for (a), (c) and [0 0 0 1] for (b), (d).

Under those conditions, the Figures 5(a) and 5(b) show a threading dislocation in the middle of the NW, which ends at the top. Both images are taken using perpendicular $g_{hki\ell}$ vectors. In addition, in the Figures 5(c) and 5(d) threading dislocations are found in the NWs and also in the GaN film. In particular, dislocations located in NWs are the continuation of the ones located in the GaN film. Moreover, point defects are observed.

Finally, the observations under this condition apparently show less threading dislocations in the NWs of the sample C2. This is a positive effect of the RTA treatment, which reduces the defect density. In addition, the quantity of threading dislocations located in the NWs is lower compared with the ones in the film, this could be a consequence of the reduced diameter of the NWs because threading dislocations could escape from the lateral NW sides.

E. High-resolution analysis

High Resolution TEM mode (HRTEM) is appropriate to observe and evaluate the crystallographic structure at atomic resolution. HRTEM images are formed using the transmitted and the scattered beam to create an interference image which is a phase contrast image. Selecting a large enough aperture, the outgoing diffracted electron waves at very low angles interfere each other given a lattice fringe pattern at the image plane corresponding to the crystallographic atomic positions of the real lattice.

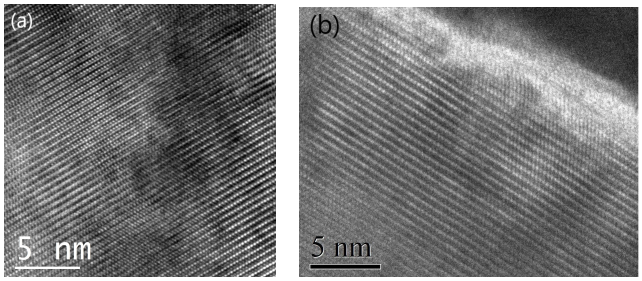

Figure 6: HRTEM images of the GaN NWs. (a) Sample C1. (b) Sample C2.

The Figures 6(a) and 6(b) are high resolution phase contrast images. Though the good quality of the lattice, some crystallographic defects have been observed and the Figure 7 is a clear example of that. In the 7(a) a threading dislocation is found, while in the 7(b) a point defect is identified.

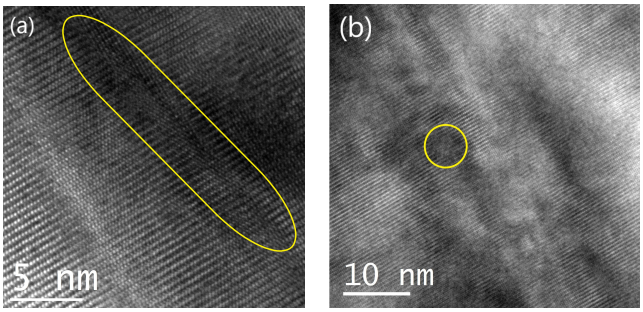

Figure 7: HRTEM images of the sample C1 showing lattice defects in the NWs: (a) threading dislocation (b) point defect.

Most of defects found in those samples are dislocations, which are a linear defect where some of the atoms are

out of position in the crystal lattice. There are two basic types: the edge dislocations and the screw ones, however it is also habitual to find mixed dislocations. Edge ones are caused by an extra half-plane of atoms introduced in the middle of a crystal, while, screw dislocations are produced when a helical path is traced around the dislocation line by the atomic planes in the crystal lattice. Usually, the threading dislocations are screw type.

Finally, the fast fourier transform (FFT) has been calculated from a HRTEM image. The FFT obtained can be interpreted as the reciprocal lattice and the resultant pattern is the Figure 8(b). If it is compared with the diffraction patterns, Figure 3(a), then, it is deduced that wurtzite crystal structure is also identified in the HRTEM images. Therefore, FFT is an alternative way to retrieve information about the reciprocal lattice to determine the crystallographic structure.

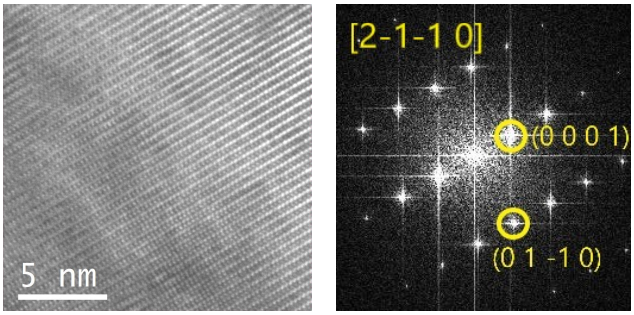

Figure 8: HRTEM image of a GaN NW of the sample C1 and its power spectrum.

IV. DISCUSSION

Threading dislocations detected in the film, Figures 5(c) and 5(d), could be a consequence of the lattice mismatches among sapphire ($a = b = 4,7606$ Å and $c = 12,994$ Å), AlN ($a = b = 3,113$ Å and $c = 4,981$ Å) and GaN ($a = b = 3,1460$ Å and $c = 5,1250$ Å) in the interfaces sapphire-AlN and AlN-GaN, which generates stress in the boundary of those materials [11]. It is also observed that most of the threading dislocations in the NW grow from the GaN film. Threading dislocations can be related with the misfit dislocations, which are a direct consequence of lattice mismatches [12]. They are caused by a missing or dangling bond in the lattice between two layers with different structural constants. Every misfit generates two threading dislocations at the ends of them, which must thread to a surface or form a loop where the two ends of the dislocation can join.

For a future study, it would be interesting to obtain the diffraction patterns in the scanning transmission electron microscope mode and study the stress distribution of the NWs by comparison with reference diffraction patterns, in order to obtain a strain distribution map along the NWs.

V. CONCLUSIONS

To summarize, the characterization of the samples has been carried out by the different operation modes of the TEM. Although some defects have been identified in the crystal, in general, the crystallographic structure observed in the GaN NWs shows a good quality. Besides, the diffraction patterns have confirmed the wurtzite structure. On the other hand, the two-beam mode has been very useful to analyse the defects which, principally, have been identified as threading dislocations and point defects. The threading dislocations detected in the NWs were the continuation of the ones found in the GaN film, therefore, they are a consequence of the strain generated in the layer-substrate interface. Finally, in relation with the RTA process, apparently, has resulted effective for the reduction of defects in the NWs.

Acknowledgments

I wish to thank my supervisors, Dr. Francesca Peiró and Gemma Martín for their help during this project. We acknowledge TEM and FIB facilities at the Technological and Scientifical Centers of the University of Barcelona (CCiT-UB) and CNM-IMB. We also acknowledge A. Georgakilas from FORTH -IESL at Heraclion, Crete, for the growth of the samples.

[1] U.K. Mishra, P. Parikh, and Y.F. Wu, Proceeding of the IEEE, 90, 2002.
[2] J. Wierer, Q. Li, D.D. Koleske, S.R. Lee and G.T. Wang, Nanotechnology, 23, 2012.
[3] H.M. Kim, Y.H. Choo, H. Lee, S.I. Kim et al, Nano Letters, 4, 2004.
[4] J.C. Johnson, H.J. Choi, K.P. Knutsen, R.D. Schaller et al, Nature Material, 1, 2002.
[5] A.L. Bugallo, M. Tchernycheva, G. Jacopin et al, Nanotechnology, 21, 2010.
[6] K.S. Im, C.H. Won, S. Vodapally, R. Caulmilone et al, Applied Physics Letters, 109, 2016.
[7] F. Yu, D. Rümmler, J. Hartmann, L. Caccamo et al, Applied Physics Letters, 108, 2016.
[8] Y. W. Jo et al., IEEE Electron Device Letters, 36, 2015.
[9] M. Schaffer, B. Schaffer and Q. Ramasse, Ultramicroscopy, 114, 2012.
[10] D.B. Williams and B.C. Carter, Transmission Electron Microscopy, Springer Verlag, 2009.
[11] A. Fontcuberta i Morral, S.A. Dayeh and C. Jagadish, Chapter Two of Semiconductor Nanowires I, Elsevier, 2015.
[12] N.G. Weimann, L.F. Eastman, D. Doppalapudi et al, Journal of Applied Physics, 83, 1998.